



HAL
open science

Carbon paramagnetic defects in silica sol-gel prepared materials.

Antonio Barbon, Silvia Gross, Eugenio Tondello, Marina Brustolon

► **To cite this version:**

Antonio Barbon, Silvia Gross, Eugenio Tondello, Marina Brustolon. Carbon paramagnetic defects in silica sol-gel prepared materials.. *Molecular Physics*, 2008, 105 (15-16), pp.2177-2183. 10.1080/00268970701747207 . hal-00513157

HAL Id: hal-00513157

<https://hal.science/hal-00513157>

Submitted on 1 Sep 2010

HAL is a multi-disciplinary open access archive for the deposit and dissemination of scientific research documents, whether they are published or not. The documents may come from teaching and research institutions in France or abroad, or from public or private research centers.

L'archive ouverte pluridisciplinaire **HAL**, est destinée au dépôt et à la diffusion de documents scientifiques de niveau recherche, publiés ou non, émanant des établissements d'enseignement et de recherche français ou étrangers, des laboratoires publics ou privés.



Carbon paramagnetic defects in silica sol-gel prepared materials.

Journal:	<i>Molecular Physics</i>
Manuscript ID:	TMPH-2007-0161.R2
Manuscript Type:	Full Paper
Date Submitted by the Author:	04-Oct-2007
Complete List of Authors:	Barbon, Antonio; University of Padova, Dip. Scienze Chimiche Gross, Silvia; CNR-ISTM Tondello, Eugenio; University of Padova, Dip. Scienze Chimiche Brustolon, Marina; University of Padova, Dip. Scienze Chimiche
Keywords:	esr, sol-gel, silica, defect, carbon



Carbon paramagnetic defects in silica sol-gel prepared materials.

Antonio Barbon¹, Silvia Gross², Eugenio Tondello¹, Marina Brustolon¹

1- Dipartimento di Scienze Chimiche, Università degli Studi di Padova and INSTM, via Marzolo, 1, I-35131 Padova, Italy

2- CNR-ISTM, Dipartimento di Scienze Chimiche, Università degli Studi di Padova and INSTM, via Marzolo, 1, I-35131 Padova, Italy

Abstract

Silica obtained by annealing in air of gels produced from the controlled hydrolysis and condensation of methacryloxypropyltrimethoxysilane (MAPTES) exhibit lorentzian and gaussian EPR signals centered at $g=2.0037$ similar to those found in coals. The number and widths of lorentzian lines depend on the annealing temperature, and are attributed to graphitic clusters of different sizes showing spin exchange. These results agree with the estimated average dimensions of the clusters at the different annealing temperatures, obtained by correlating the carbon content with the number of spins. Inhomogeneous components have been identified by using the echo-detected EPR method and are attributed to smaller isolated clusters. These latter analyzed by ESEEM and HYSCORE show strong signals at the free nuclear frequencies of ^{13}C and ^1H nuclei only, and hyperfine interactions of 5 MHz with a ^{13}C nucleus.

Introduction

Silica is a low-cost material that is extensively used in many technological applications because of its versatility [1]. An important employ of the substance is its use as inert matrix for the dispersion or the support of active species in very different application fields like catalysis [2] or optics [3-4]. The requirements asked to the prepared materials are very different, depending on their use. A convenient method for the production of many silica-based materials, both bulk or powders, is the sol-gel method [5]; it allows the formation of whole inorganic or inorganic-organic hybrid materials

1
2
3 [6-7], it involves low temperatures and mild processing conditions and it is economically
4 advantageous with respect to other production processes like MCVD (Modified Chemical Vapor
5 Deposition) or VAP (Vacuum Assisted Process) methods [8]. Silica gels are produced by hydrolysis
6 and condensation of silicon alkoxides [5-7]. Annealing of gels at different temperatures leads to loss
7 of hydrogen atoms and to the thermal decomposition of most of the organic parts [9] for
8 temperatures higher than 600° C. The annealing process leaves in the silica matrix a carbon content,
9 which depends on the preparation procedure, in particular on the oxidation conditions [10], and
10 decreases in quantity on increasing the calcination temperature. The characterization of these
11 carbon impurities is important, as the presence of active species or sites, also at very low
12 concentrations, can dramatically change the macroscopic properties of the material with respect to
13 those of the pure silica. For example, the presence of ZrO₂ in the material enhances its thermal
14 stability and insulating properties [11], but if a small quantity of carbon is present, the material can
15 even be a conductor [12].

16
17 In this paper we report a cw and pulsed X-band EPR study on the paramagnetic carbon clusters
18 formed in the synthesis of silica powders, prepared by the annealing of the gel obtained from the
19 controlled hydrolysis and condensation of methacryloxypropyltrimethoxysilane (MAPTES). This
20 organically functionalized silane, bearing a polymerisable moiety, is a well known sol-gel precursor
21 and it has been extensively used previously by some of us [13-15] as precursor for preparing
22 different inorganic-organic hybrid materials based on the embedding of transition metal oxocluster
23 in a silica matrix. Furthermore, its hydrolysis and condensation behaviour has been thoroughly
24 investigated and optimised in terms of time and composition of the starting solution [13]. In this
25 paper, our aim was to study the presence of paramagnetic defects and their evolution upon
26 annealing of the silica at different temperatures. We have been able to detect strong EPR signals
27 typical of carbon clusters, and we have shown that the materials formed during the calcination can
28 be considered as a “composite” materials consisting of traces of a graphite-like carbon phase in the
29 inorganic oxidic component, with a composition depending on the annealing temperature. Four
30 samples of MAPTES-derived gels annealed at different temperatures have been studied, and, as a
31 reference, the gel obtained by a typical tetraalkoxysilane, extensively used in sol-gel synthesis of
32 silica-based materials, in which four instead of three alkoxy groups undergo hydrolysis and
33 condensation.
34
35
36
37
38
39
40
41
42
43
44
45
46
47
48
49
50
51
52
53
54
55
56
57
58
59
60

Pulse-EPR Methods

The following spin Hamiltonian has been used, taking account of the Zeeman electron and nuclear interactions and of the hyperfine dipolar coupling:

$$H = \mu_B \mathbf{S} \cdot \mathbf{g} \cdot \mathbf{B} + \sum_j [g_{n,j} \beta_{n,j} \mathbf{I}_j \cdot \mathbf{B} + \mathbf{S} \cdot \mathbf{T}_j \cdot \mathbf{I}_j] \quad (1)$$

where \mathbf{S} and \mathbf{I} are the electron and nuclear magnetic moment operators, \mathbf{g} and \mathbf{T}_j are the g and the hyperfine tensors [16].

In a collection of paramagnetic centers in thermal equilibrium included in a solid powder sample, a distribution of orientations leads generally to inhomogeneously broadened Gaussians in the cw-EPR spectrum. A fast dynamics of the electron spins, as a sufficiently strong spin exchange, can average the magnetic interactions, and in this case exchange narrowed homogeneously broadened EPR Lorentzian lines appear. In the cw-EPR spectrum, homogeneously and inhomogeneously broadened lines overlap, and it can be impossible to disentangle the components. Pulsed EPR allows to separately detect the two types of lines, as homogeneous components give rise to Free-Induction Decay (FID) generated by a single $\pi/2$ pulse, whereas inhomogeneous broadened lines dephase faster and can be detected only in the refocused spin echo. Echo-EPR spectra of the inhomogeneous components are obtained by recording the primary echo intensity ($\pi/2-\tau-\pi-\tau$ -echo) while sweeping the magnetic field. The spectral resolution of this technique is determined by the reverse of the integration time window used to record the intensity and/or by the pulse lengths.

The Electron Spin Echo-Envelope Modulation (ESEEM) can be obtained from the 3-pulse $\pi/2-\tau-\pi/2-T-\pi/2-\tau$ -echo sequence by recording the echo intensity while varying the time T [17-18]. From the simulation of the time profile or of its Fourier Transform the determination of the hyperfine tensor and the nuclear frequency can be obtained.

Hyperfine sublevel correlation (HYSCORE) enhances the spectral resolution of ESEEM by extension of the spectrum into two dimensions. The pulse sequence is $\pi/2-\tau-\pi/2-t_1-\pi-t_2-\pi/2-\tau$ -echo and the spectrum is obtained by recording the echo intensity while varying the t_1 and t_2 delay times [19].

Experimental

Materials

Methacryloxymethyltriethoxysilane (purchased from Gelest), anhydrous tetrahydrofuran were used as received and then stored under argon. Tetraethylorthosilicate (TEOS) was purchased by Aldrich. The polymerisation thermal initiator dibenzoylperoxide was purchased by Aldrich.

Preparation of the samples

The silica gels were prepared starting from methacryloxymethyltriethoxysilane, as elsewhere extensively reported [13-14]. After polymerisation, the silica based gels were dried under vacuum at 70° C for 12 h to eliminate the residual solvent. The prepared gels were thermally annealed at 500°, 700°, 900°, 1000° C for 4 h in air to promote pyrolysis of the organic components and their conversion to the corresponding silica oxide. Powder samples were obtained.

In the Table 1 and in the following, the labels “MAPTES_XX” indicate specimens prepared by using the methacryloxymethyltriethoxysilane as silica source, while the number indicates the final annealing temperature.

The reference gel sample (TEOS_1000) was prepared by acid-catalyzed hydrolysis and condensation of TEOS by using a TEOS:EtOH: H₂O:HCl molar ratios of 1:4:4:0.01, by following the procedure described by Aguilar et al. [20]. The gel was then calcined at 1000° C for 4 hours.

EPR measurements

An X-band Bruker ELEXYS spectrometer with a dielectric resonator was used for the continuous-wave EPR (cw-EPR) experiment and pulse-EPR experiments. The cavity was inside a CFR934 Oxford cryostat cooled with liquid helium or nitrogen. Hahn echo experiments were run with low Q. Pulses of 16 and 32 ns were used.

Samples were not degassed. For one sample, removing of oxygen by vacuum pumping (10⁻⁵ bar for 4 hour) produced no effects on the cw-EPR spectrum.

The number of spins has been measured by comparing the double integral of the cw-EPR spectra of weighted samples with respect to a manganese standard (MnO in CaO) [21]. All the measurements were realized with the same Q-factor of the cavity (±10%) and at the same frequency (±1%) indicative of the same loading of the cavity. The estimated error is 30%.

Results

MAPTES

We have studied by cw and pulsed EPR the samples calcined at different temperatures reported in Table 1.

Table 1.

Linewidths of lorentzian lines at $g = 2.0037$ obtained by the simulations of the room temperature cw-EPR spectra for MAPTES calcined at different temperatures. Carbon and hydrogen contents determined by elemental analysis. Number of spins per gram from quantitative EPR. Estimated average radii of the clusters, see text.

Sample	LW ^b , % in parenthesis			%H	%C	N spins/g	r/nm
MAPTES_500 ^a	0.03			0.98	2.53	$3 \cdot 10^{16}$	5.6
MAPTES_700	0.04 (40)	0.13 (60)		0.15	0.40	$1.7 \cdot 10^{17}$	1.8
MAPTES_900	0.04 (50)	0.16 (50)		0.10	0.29	$1.4 \cdot 10^{18}$	0.79
MAPTES_1000	0.06 (30)	0.15 (55)	0.41 (15)	0.05	0.14	$3.2 \cdot 10^{18}$	0.47

a. Only the narrow single lorentzian line is reported, see text.

b. Half-width in mT.

cw-EPR and FT-EPR

The spectra obtained at room temperature are shown in figure 1 in the integrated form, together with their simulations. All the spectra are given by one or more lorentzian lines centered at $g = 2.0037$, whose linewidths are reported in table 1. It should be noted that the spectra cannot be fitted satisfactorily by gaussian or dysonian lines. The spectrum of MAPTES_500 is given also by three intense and broader lines with different g -values that we attribute to radicals trapped in organic residues left by the relatively low combustion temperature (500°C). Other studies carried out on analogous materials [14] have evidenced as at 500°C uncombusted organic material is present in the samples. This is confirmed by the high carbon content in this sample (see Tab 1). These signals have not been analyzed further.

A FT-EPR investigation on the sample MAPTES_1000 shows a FID corresponding to the same homogeneously broadened lines found in cw-EPR, see figure 1.

As can be seen from table 1, the lines become broader and increase in number for higher calcination temperatures. This effect leads to a larger uncertainty in the fitting results. In particular in MAPTES_1000, the presence of inhomogeneously broadened Gaussian components cannot be ruled out on the basis of the cw-EPR results.

The number of spins per gram of silica has been obtained for the four samples, and it is reported in Table 1. The increase of number of spins and the decrease of carbon content on increasing the annealing temperature indicate a progressive reduction of the carbon cluster size, in agreement with the lineshape EPR results and with previously reported studies on samples prepared by the same route [13-14]

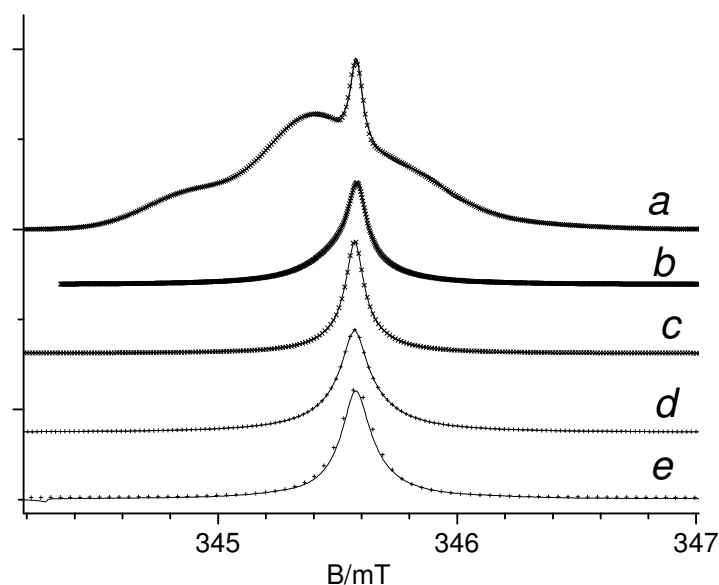


Fig. 1 Integrated cw-epr spectra at room temperature of MAPTES samples calcined at different temperatures *a*: 500° C, *b*: 700° C, *c*: 900° C, *d*: 1000° C and *e*: FT-EPR spectrum of sample calcinated at 1000° C. The crosses show the simulated spectra given by a superposition of Lorentzian lines. The parameters are given in Table 1.

Electron Spin Echo

To look for fast dephasing inhomogeneously broadened components, we have studied MAPTES_1000 also by two pulses Electron Spin Echo (ESE). We have detected a weak spin echo signal. The echo decays monoexponentially giving a phase memory time $T_M = 1100$ ns at room temperature but for the first delay time (200 ns). This can be explained by the inhomogeneity of the

sample, for which we expect a distribution of phase memory times, with the shortest ones due to strongly interacting paramagnetic centers. The EchoEPR spectrum, obtained recording the integrated echo by sweeping the magnetic field, shows two Gaussian lines with widths 0.17 mT and 0.41 mT (see figure 2) and relative weights of 1:2 (2:3 for spectrum *a*).

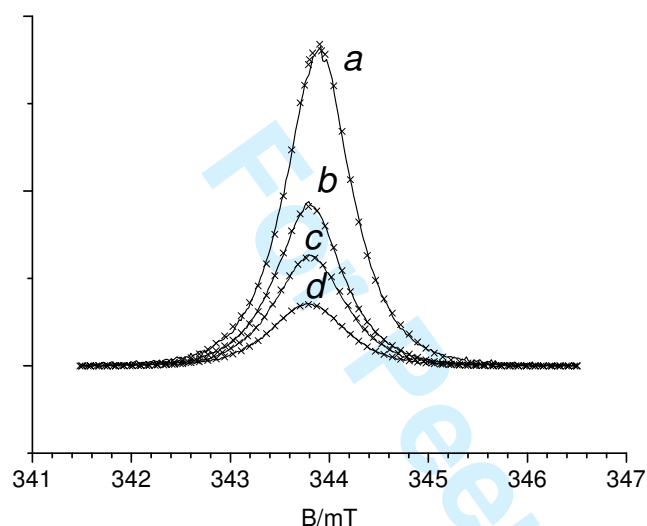


Figure 2. Echo-detected EPR spectrum at room temperature of MAPTES_1000 for different delays τ between the pulses: from the more intense line, *a*. $\tau=200$ ns, *b*. $\tau=300$ ns, *c*. $\tau=600$ ns, *d*. $\tau=1200$ ns. The echo sequence was 276- τ -572 ns; for *a*. the $\pi/2$ pulse was reduced to 176 ns. The simulated spectra are given by two overlapping Gaussians and are shown by the crosses. The linewidths of the fitting Gaussians for the spectra. are 0.17 mT and 0.41 mT.

A 3-pulse echo experiment shows a weak modulation of the echo decay (ESEEM). The FT of the modulation signal after subtraction of the exponential decay is reported in Fig.3. The frequencies corresponding to the free nuclear resonances for ^{13}C (1% natural abundance), ^1H and ^{29}Si (5% natural abundance) are indicated. As it can be seen, strong signals at the free nuclear frequencies are present for ^{13}C and ^1H , and a much weaker one for ^{29}Si . The other lines in the spectrum can be attributed to ^{13}C nuclei coupled to the paramagnetic centers, on the basis of the simulation reported in the right part of figure 3. The simulation is based on a dipolar hyperfine interaction with a ^{13}C with principal values of -1.5 , -3.5 and 5 MHz, and an isotropic interaction of 5 MHz. The experimental spectra show broader lines, corresponding, as it can be expected, to a distribution of hyperfine interactions with ^{13}C nuclei. It should be noted that simulations based on the hypothesis of a coupling with ^{29}Si nuclei show a bad agreement with the experimental spectrum.

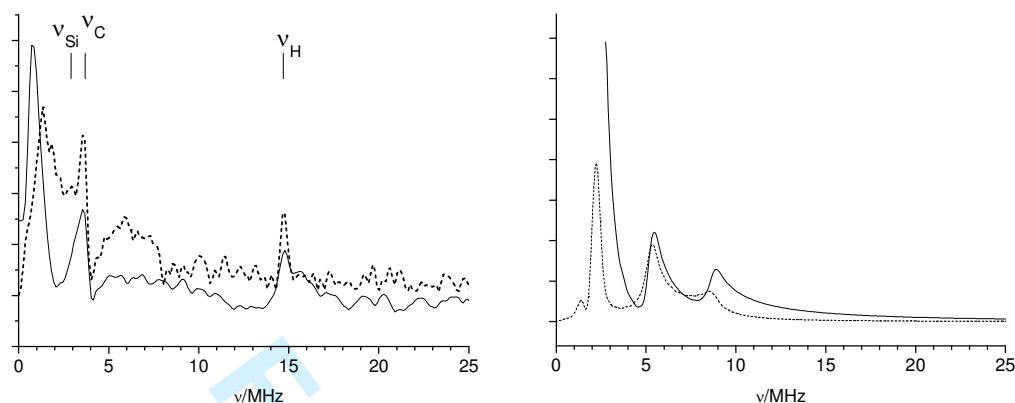


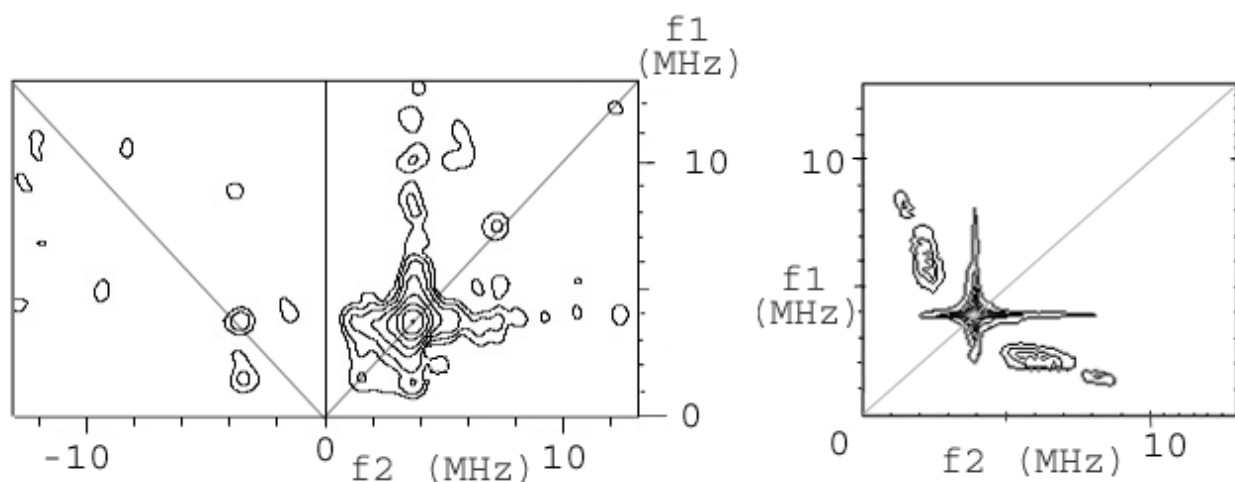
Figure 3. Fourier Transform of the three pulses ESEEM signal of MAPTES_1000 at room temperature. Left: Experimental spectra obtained for delays between the first and the second pulse of 140 ns (dashed line) and 220 ns (continuous line). The indicated Larmor frequencies of the three nuclei correspond to a field of 345.6 mT.

Right: Simulated spectra for the same delays as above obtained by assuming a hyperfine interaction with a ^{13}C ($I = 1/2$, 1% natural abundance) with principal values of -1.5 , -3.5 and 5 MHz, and an isotropic interaction of 5 MHz.

An improvement in the spectral resolution at the low frequencies has been obtained by HYSORE (see fig. 4). The spectrum shows the presence of nuclei, mainly ^{13}C , with various hyperfine tensors, as expected for this heterogeneous sample. The most intense diagonal peak corresponds to free ^{13}C (3.7 MHz), but other much less intense peaks are present at 1.5 , 7.4 and 12.1 MHz, the second corresponding to twice the free carbon frequency. For the off diagonal peaks the most evident features are the perpendicular ridges crossing star-like at the free carbon frequency. They form an asymmetric feature that span from 1 up to about 8 MHz, but isolated peaks can be detected up to 12 MHz. According to [22], this feature indicates the presence of two sets of coupled ^{13}C nuclei, with different hyperfine tensors. Four peaks are present in the first and second quadrant at around $(\pm 10.5, \mp 3.5)$ MHz. On the basis of the resonant frequencies only, these peaks might belong to strongly coupled Si or C nuclei, as the distance between them is 9 MHz, which is about twice the nuclear frequency of both nuclei. Other paired peaks are those at $(2.0, 4.5)$ MHz, overlapping the free-carbon peak in the first quadrant, and at $(\pm 1.5, \mp 3.7)$ MHz in the second.

The simulation, also shown in figure 4, has been obtained by taking into account two sets of coupled ^{13}C nuclei, one with the hyperfine parameters used in Fig. 3, the other of weakly coupled carbon atoms. As one can see the asymmetric shape of the star-like feature is well reproduced. The off diagonal peaks evident in the simulation are also present but much less intense in the

1
2
3 experimental spectrum. It is worth noting that a simulation based only on weakly coupled ^{13}C
4 nuclei would not show the remarkable star-like feature, and therefore the HYSORE results
5 confirm the presence of strongly coupled ^{13}C nuclei.
6
7



25
26
27
28
29
30
31
32
33
34
35
36
37

Figure 4. Left: HYSORE powder spectrum of MAPTES_1000 at room temperature with $\tau=136$ ns. Right: simulation of the HYSORE spectrum by using two sets of coupled nuclei: a ^{13}C with hyperfine principal values of -1.5, -3.5 and 5 MHz and an isotropic interaction of 5 MHz, and a set of weakly coupled ^{13}C 's. The simulation shows only the real part of the echo intensity.

38 39 40 41 42 43 44 45 46 47 48 49 50 51 52

TEOS_1000

We studied a sample prepared from TEOS, and calcined at 1000°C . The cw-EPR spectrum (data not shown) has been nicely fitted with two superimposed lorentzian lines, with the same g factor as the lines observed in MAPTES_1000, and widths 0.08 and 0.24 mT. Like for MAPTES_1000 we used Electron Spin Echo spectroscopy to detect inhomogeneously-broadened components. The EchoEPR spectrum shows two Gaussian lines with widths 0.55 and 1.14 mT. The similarities observed can be ascribed to the similar compositional and structural features of the two samples.

53 54 55 56

Discussion

57
58
59
60

Let us summarize and briefly discuss the results obtained up to now. The combustion at relatively low temperatures (500°C) produces a carbon content much higher than in the other cases (see Table 1) and an EPR spectrum which is substantially different from that of the other MAPTES samples, that is attributed to organic incombusted radicals. Samples annealed at higher temperatures

1
2
3 show all similar spectra, with Lorentzians of different widths, all superimposed at a very similar g
4 value (2.0037 ± 0.0002). For MAPTES_1000 moreover, the ESE spectra have shown also the
5 presence of weak Gaussian lines of different widths underneath the Lorentzian ones. This kind of
6 multi-component EPR spectrum at this g value is typical of paramagnetic centers in coals, and it has
7 been attributed to unpaired electrons on aromatic and hydroaromatic carbon clusters of different
8 size [23]. The similarity of the paramagnetic centers we observe with those observed in carbon-
9 based materials is confirmed by our ESEEM results, that show a much stronger modulation of the
10 echo due to hyperfine interactions with ^{13}C atoms and protons, compared to the modulation of ^{29}Si ,
11 see figure 3.
12

13
14 Let us discuss the effects on the EPR spectra expected for unpaired electrons in such clusters,
15 depending on the size and number of the clusters, on the number of unpaired spins and on the
16 mobility of the charges. Several factors can bring to a narrowing of the spectrum of an unpaired
17 electron localized on a hypothetical isolated single monomer radical of a definite size. First of all
18 the width of the EPR spectrum is reduced if the size of the π delocalization increases, as each spin is
19 affected by an averaged hyperfine interaction with a narrower statistical distribution. In this case
20 Gaussian line shapes with temperature independent spectral characteristics are expected [24].
21 Therefore, for isolated paramagnetic centers we should expect inhomogeneously broadened
22 Gaussians with a width decreasing on increasing the cluster dimension.
23

24
25 The electron transfer between near clusters brings also to an averaging of magnetic interactions, by
26 a process similar to the chemical exchange in solution, $A + A^- \rightarrow A^- + A$. In this case the spectral
27 lines are generally non-Gaussian [24], and the efficiency of the narrowing increases with the
28 number of near partially overlapping clusters.
29

30
31 Other processes leading to line narrowing are based on spin exchange between adjacent
32 paramagnetic centers. The interaction between two unpaired electrons with overlapping spin
33 distributions produces fluctuations of the spin states. A further spin exchange can proceed via the
34 collisions of unpaired electron spins for electron transfer. Spin exchange gives rise to line narrowed
35 Lorentzians when the process is fast enough to average the hyperfine interactions. Its efficiency is
36 enhanced on increasing the number of spins in close proximity, and on increasing the size of the
37 clusters. In fact for larger clusters the extent of hyperfine coupling is reduced, and the clusters are
38 more overlapping.
39

40
41 On the basis of this complex model, we can draw some evidences from the experimental results at
42 different annealing temperatures. As seen in table 1, on increasing the annealing temperature the
43 carbon content decreases, the number of spins increases, and broader Lorentzian lines appear. Large
44 clusters of carbon atoms with unpaired electrons in such close proximity to give rise to strong spin
45
46
47
48
49
50
51
52
53
54
55
56
57
58
59
60

1
2
3 exchange are therefore formed at the lower annealing temperatures. The lower ratio between
4 number of spins and carbon content can be explained also by the larger size of the clusters, each
5 bearing a single unpaired electron.
6
7

8
9 A rough hint on the average size of the clusters can be obtained from the following model. By
10 assuming that each cluster bears an unpaired electron, the number of clusters in a sample is equal to
11 the number of spins. If the clusters had all the same size, and by assuming that the density is similar
12 to that in graphite ($\sim 2.1 \text{ g/cm}^3$), we can obtain the volume of the clusters from the ratio between the
13 carbon content (expressed in volume/g) and the spin number. In this way we obtain the average
14 radii for spherical clusters reported in Table 1.
15
16
17
18

19 As the annealing temperature is increased, the average cluster size decreases, and moreover they are
20 progressively more separated and less close to each other, as the carbon contents is less. Broader
21 Lorentzians appear, due to a weaker spin exchange. Isolated unpaired electrons in this model give
22 rise to the inhomogeneously broadened Gaussians detected by electron spin echo experiments, with
23 inhomogeneous linewidths depending on the size of the clusters. The homogeneous linewidths of
24 the contributing Lorentzians can be obtained from the dephasing rate of the echo, T_M^{-1} . In fact in
25 general the dephasing rate depends on T_2^{-1} , the spin-spin relaxation of the homogeneous
26 components, and on collective processes as spin diffusion or instantaneous diffusion. Since these
27 latter two contributions are expected to be relatively unimportant for the present diluted spin
28 systems, we can assume $T_M^{-1} \sim T_2^{-1}$. The measured value corresponds to a linewidth smaller than
29 0.01 mT. Therefore the homogeneous components of the inhomogeneous line are narrower than the
30 lines in Table 1. This is not surprising, as the exchange narrowed Lorentzians detected by cw-EPR
31 are expected to show nevertheless a residual linewidth due to an incomplete averaging of the
32 magnetic interactions.
33
34
35
36
37
38
39
40
41
42
43

44 As shown by the ESEEM and HYSCORE spectra the inhomogeneously broadened EPR lines
45 correspond to localized electrons, coupled to ^{13}C nuclei. The determined hyperfine tensor can give a
46 hint on the degree of delocalization of the unpaired electron in some of the clusters, by comparing it
47 with the values measured for example for some C_{60} derivatives. For the radical anion of N-methyl-
48 3,4-fulleropyrrolidine [25] the isotropic ^{13}C hyperfine coupling constants are in the range 2-7 MHz,
49 therefore of the same order of magnitude of that measured in this case (5 MHz). A hypothesis of
50 carbon clusters of the size of a C_{60} molecule is in agreement with the average radius of the cluster
51 for MAPTES_1000 reported in Table 1, similar to that of C_{60} fullerenes.
52
53
54
55
56
57

58 The comparison between the results obtained for MAPTES and TEOS brings to conclude that the
59 same type of carbon clusters are formed in the two cases, as could be reasonably expected by
60 considering the similar chemical nature of the two materials and the similar synthesis procedure

used for their preparation. The large inhomogeneous linewidth of one of the echoEPR detected Gaussians (1.14 mT) might be attributed to an electron-electron dipolar interaction between non-exchanging localized electrons. Further studies would be necessary for a more detailed analysis of the differences of carbon clusters in the two samples.

Conclusions

The annealing of the gels of MAPTES gives silica with clusters of carbon atoms, showing EPR spectra very similar to those detected in coals. From this similarity we deduce that, as in coals, the clusters are graphitic. From the cw and pulsed EPR experiments we get the information that i.) all the clusters are very similar, only their sizes and average reciprocal distances vary; ii) the unpaired electrons have hyperfine interactions with a number of ^{13}C and ^1H nuclei, and only with very few ^{29}Si nuclei.; iii) the large majority of the unpaired electrons are exchanging fast their spins, but some of them are localized and not exchanging.

From the number of spins measured by quantitative EPR, and the carbon content from chemical analysis, the average size of the clusters can be obtained. It results that the average size decreases on increasing the annealing temperature. This is in agreement with the observation that broader EPR lines appear as the temperature is increased, as expected if the clusters are decreasing in size. For the highest annealing temperature (1000° C), the average diameter of the clusters is 1 nm, corresponding to a π delocalization of a dimension similar to that on C_{60} . This observation is in agreement with the hyperfine interaction with a ^{13}C nucleus measured by ESEEM, which is in the range of those obtained for the radical anions of C_{60} derivatives .

Acknowledgment

This work was supported in part by the Italian Ministry of University and Research via the PRIN program 2005 “Architetture molecolari organizzate su matrici inorganiche ed ibride”.

Bibliography

- [1] R. K. Iler, *The Chemistry of Silica*, ed. J. Wiley & Sons, New York (1979).
- [2] T. Lopez, F. Tzompantzi, J. Navarrete, R. Gomez, J.L. Buldú, E. Muñoz, O. Novaro, *J. Catal.* **181**, 285 (1999).
- [3] F. Chaumel, H. Jiang, A. Kakkar, *Chem. Mater.* **13**, 3389 (2001).

1
2
3
4
5
6
7
8
9
10
11
12
13
14
15
16
17
18
19
20
21
22
23
24
25
26
27
28
29
30
31
32
33
34
35
36
37
38
39
40
41
42
43
44
45
46
47
48
49
50
51
52
53
54
55
56
57
58
59
60

- [4] P. Innocenzi, E. Miorin, G. Brusatin, A. Abbotto, L. Beverina, G. A. Pagani, M. Casalboni, F. Sarcinelli, R. Pizzoferrato, *Chem. Mater.* **14**, 3758 (2002).
- [5] C.J Brinker, G.W Scherer, *Sol Gel Science: The Physics and Chemistry of Sol-Gel Processing*, ed. Academic Press Inc., San Diego (1990).
- [6] U. Schubert, N. Hüsing, *Synthesis of Inorganic Materials*, Wiley VCH, Weinheim, 2nd Edition (2005).
- [7] L.L. Lench, J.K. West, *Chem. Rev.*, **90**, 33 (1990).
- [8] K. Susa, I. Matsuyama, T. Suganuma, *Elec. Lett.* **18**, 499, (1982).
- [9] A. A. Wolf, E.J. Friebele, D.C. Tran, *J. non-Cryst. Solids* **71**, 345 (1985).
- [10] C. G. Pantano, A. K. Singh, H. Zhang, *J. Sol-Gel Sci. Technol.* **14**, 7 (1999).
- [11] D. A. Nuemayer, E. Cartier, *J. Appl. Phys.* **90**, 1801 (2001).
- [12] V. G. Pol, S. V. Pol, P. P. George, B. Markovskiy, A. Gedanken, *J. Phys. Chem. B*, **110**, 13420 (2006).
- [13] L. Armelao, H. Bertagnolli, S. Gross, V. Krishnan, U. Lavrencic-Stangar, K. Müller B. Orel, G. Srinivasan, E. Tondello, A. Zattin, *J. Mater. Chem.*, **15**, 1954 (2005).
- [14] L. Armelao, S. Gross, K. Müller, G. Pace, E. Tondello, O. Tsetsgee, A. Zattin, *Chem. Mater.*, **18**, 6019 (2006).
- [15] L. Armelao, H. Bertagnolli, D. Bleiner, M. Groenewolt, S. Gross, V. Krishnan, C. Sada, U. Schubert, E. Tondello, A. Zattin, *Adv. Funct. Mater.* **17**, 1671, (2007).
- [16] N.M. Atherton, *Principles of ESR* Ellis Horwood and Prentice Hall, London, **1993**.
- [17] M. Brustolon, A. Barbon in *EPR of Free Radicals in Solids*; A. Lund, M. Shiotani; *Editor* vol 10 of series *Progress in Theoretical Chemistry and Physics*, Editors-in-chief J. Maruani and S. Wilson Publisher; Kluwer Academic, Dordrecht, (2003).
- [18] W.B. Mims, *Phys. Rev. B*, **5**, 2409 (1972).
- [19] P. Hofer, A. Grupp, H. Nebenfuhr, M. Mehring *Chem. Phys. Lett.*, **136**, 279 (1986).
- [20] D. H. Aguilar, L. C. Torres-Gonzalez, L. M. Torres-Martinez, T. Lopez, P. Quintana *J. Solid State Chem.* **158**, 349 (2001).
- [21] C.P. Poole, *Electron Spin Resonance: A Comprehensive Treatise on Experimental Techniques*, 2nd Edition, Dover (1997).
- [22] A. M. Tyryshkin, S. A. Dikanov, D. Goldfarb, *J. Magn. Res. A*, **105**, 271 (1993).
- [23] M. Krzesin´ska, B. Pilawa, S. Pusz *Energy & Fuels*, **20**, 1103 (2006).
- [24] N. Srivatsan, S. Weber, D. Kolbasov, J. R. Norris *J. Phys. Chem. B*, **107**, 2127 (2003).
- [25] M. Brustolon, A. Zoleo, G. Agostini, M. Maggini, *J. Phys. Chem.*, **102**, 6331 (1998).